Zhang et al. Nanoscale Research Letters (2019) 14:23
https://doi.org/10.1186/s11671-019-2860-y

Nanoscale Research Letters

NANO EXPRESS

A High-Accuracy AlGaN/GaN Reverse Blocking CRD (RB-CRD) with Hybrid Trench Cathode

Anbang Zhang*, Qi Zhou*, Chao Yang, Yuanyuan Shi, Wanjun Chen, Zhaoji Li and Bo Zhang*

Abstract

An AlGaN/GaN lateral reverse blocking current regulating diode (RB-CRD) with trench Schottky anode and hybrid trench cathode has been proposed and experimentally demonstrated on silicon substrate. The Schottky barrier diode (SBD) integrated in the anode exhibits a turn-on voltage of 0.7 V and a reverse breakdown voltage of 260 V. The hybrid trench cathode acts as a CRD, which is in series connection with the anode SBD. A knee voltage of 1.3 V and a forward operation voltage beyond 200 V can be achieved for the RB-CRD. The RB-CRD is capable of outputting an excellent steady current in a wide temperature range from 25 to 300 °C. In addition, the forward regulating current exhibits small negative temperature coefficients less than − 0.152%/°C.

Keywords: AlGaN/GaN heterostructure, Reverse blocking current regulating diode (RB-CRD), Schottky barrier diode (SBD)

Background

Wide bandgap semiconductors have attracted a considerable attention for the next generation of high-power, high-frequency, and high-temperature devices. GaN is one of the most promising wide bandgap semiconductors due to its superior properties such as large bandgap, high electron mobility, and high critical electric field [1–5]. In addition, due to the combination of spontaneous polarization and piezoelectric polarization, a high-density two-dimensional electron gas (2DEG) can be achieved at the AlGaN/GaN heterointerface. Such excellent properties enable the AlGaN/GaN-based power devices to operate with a low on-resistance while maintaining a high breakdown voltage. GaN-on silicon (GaN-on-Si) platform [6–8] has been regarded as the most promising technology towards high-performance and low-cost power devices, owing to the availability of large-diameter silicon wafers and the compatibility with the existing-matured CMOS fabrication process. Up to date, a variety of power devices [9–16] have been demonstrated on AlGaN/GaN-on-Si and some of them are commercially available. At the same time, the development of AlGaN/GaN device with new functionality may expand the application potential of AlGaN/GaN-on-Si, which is beneficial for boosting the extensive commercialization of AlGaN/GaN technology.

As presented in Fig. 1a, in this work, a new type device termed as reverse blocking current regulating diode (RB-CRD) was experimentally demonstrated on AlGaN/GaN-on-Si. The RB-CRD features a trench Schottky anode and a hybrid trench cathode. A trench Schottky barrier diode (SBD) is formed at the anode while a CRD is achieved in the hybrid trench cathode. The RB-CRD can be regarded as a SBD in series connection with a CRD. A typical application of the RB-CRD is battery charging as shown in Fig. 1b. In the aforementioned battery charging circuit, the CRD acts as a constant current source, which output a constant current to charge the battery [17–19] regardless of the forward voltage fluctuation between the input and the battery. If the input voltage falls below the battery voltage, the reverse biased SBD in the circuit will prevent the battery from discharging.

Methods

The epitaxial AlGaN/GaN heterostructure used for fabricating the RB-CRDs was grown on 6-in (111) silicon

* Correspondence: anbangzhang@outlook.com; zhouqi@uestc.edu.cn; zhangbo@uestc.edu.cn
School of Electronic Science and Engineering, State Key Laboratory of Electronic Thin Films and Integrated Devices, University of Electronic Science and Technology of China, Chengdu 610054, China

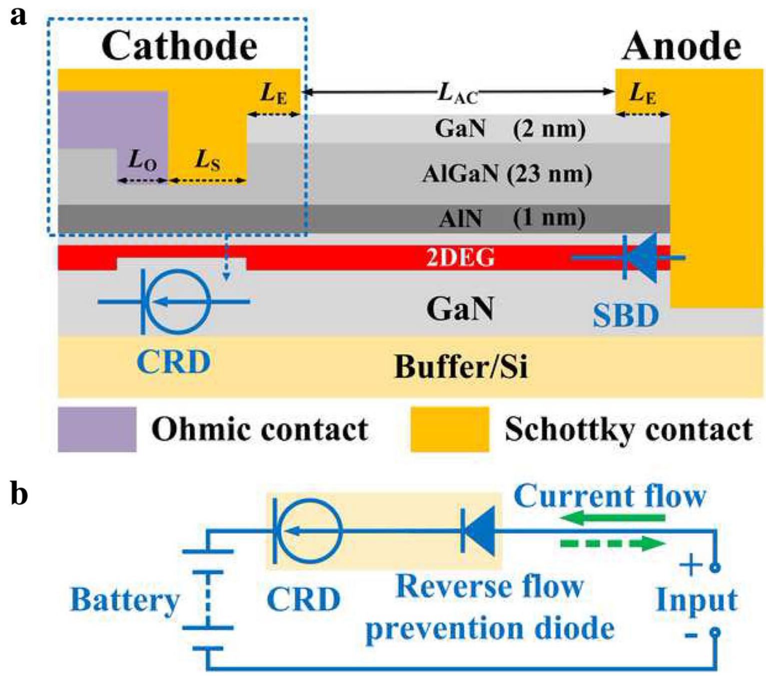

Fig. 1 a Schematic cross section of the RB-CRD. **b** Circuit diagram of battery charging using the RB-CRD

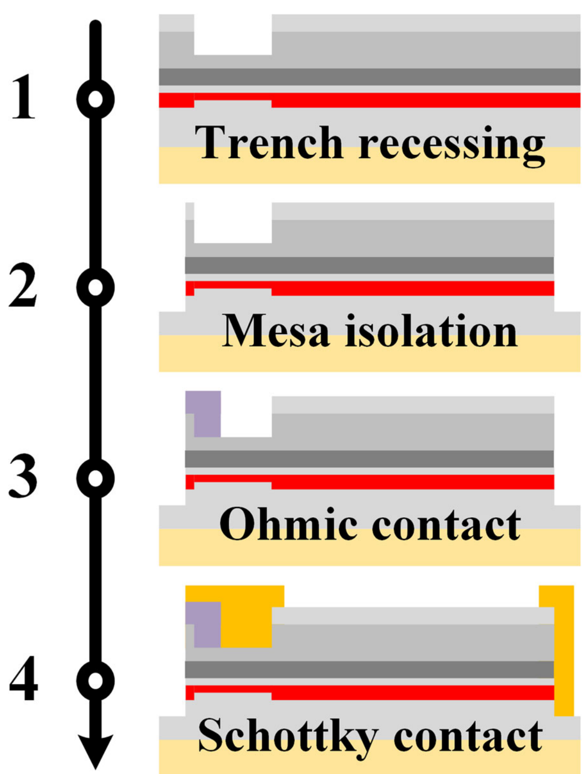

Fig. 2 Manufacturing process flow of the RB-CRD

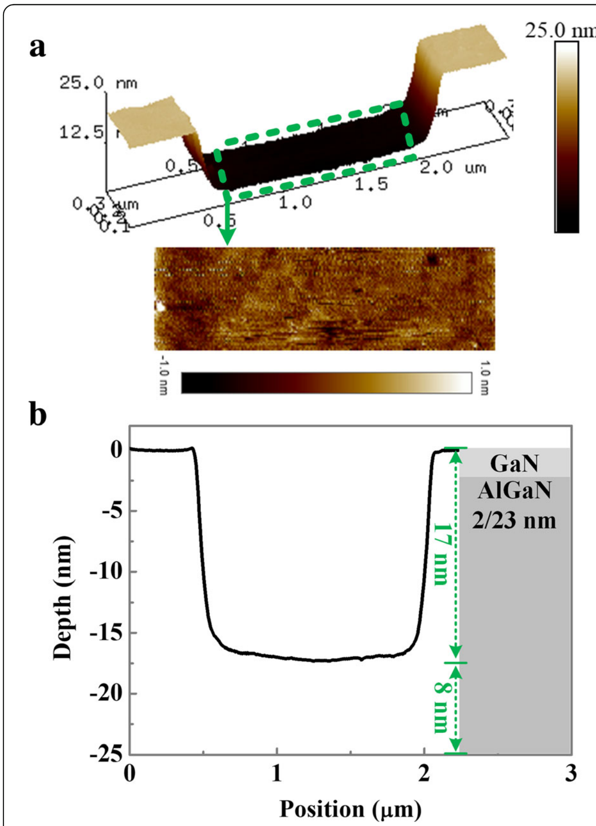

Fig. 3 a AFM images of the cathode trench. **b** Height profile taken from the cathode trench substrate by metal organic chemical vapor deposition (MOCVD). The epitaxial layers consist of 2-nm GaN cap, 23-nm AlGaN barrier, 1-nm AlN interlayer, 300-nm GaN channel, and 3.5-μm buffer. The Hall effect measured density and mobility of the 2DEG were 9.5×10^{12} cm^{-2} and 1500 cm^2/V·s, respectively. The device fabrication process is shown in Fig. 2. First, a shallow trench (see Fig. 3) was etched in the cathode of the RB-CRD by a low power Cl_2/BCl_3-based inductively coupled plasma (ICP) etching technique. An etching rate of 7 nm/min was observed using the developed etching recipe with a RF power of 20 W, an ICP power of 60 W, a Cl_2 flow of 5 sccm, and a BCl_3 flow of 10 sccm. Then, mesa isolation with a depth of 300 nm was formed using the same ICP etching technique to disconnect the devices. The anode trench was accomplished by this process simultaneously. After that, the Ti/Al/Ni/Au (20/150/55/60 nm nm) metal stacks were deposited by the electron beam evaporation, followed by the rapid thermal annealing at 880 °C for 35 s in N_2 ambient. The ohmic contact resistance of 1.1 Ω mm and sheet resistance of 400 Ω/square were extracted by the transmission line method. Finally, the device fabrication process ended up with the Ni/Au (50/300 nm) Schottky metal stack deposition. The distance between the anode and cathode (L_{AC}) is 4 μm. The lengths of the ohmic contact (L_O) and the Schottky contact (L_S) in the cathode trench are 0.5 μm and 1 μm, respectively. The extended overhang (L_E) of the Schottky contact is 0.5 μm.

Results and Discussion

Figure 3a shows the 3D atomic force microscope (AFM) image of the fabricated cathode trench. The surface roughness of the bottom of the cathode trench is 0.3 nm. Such a small surface roughness is beneficial for the following metal-semiconductor contact. As shown in Fig. 3b, with a 17-nm depth cathode trench recessing, the 8-nm AlGaN barrier layer remains in the cathode trench region. Such a remaining AlGaN barrier layer enables that the 2DEG

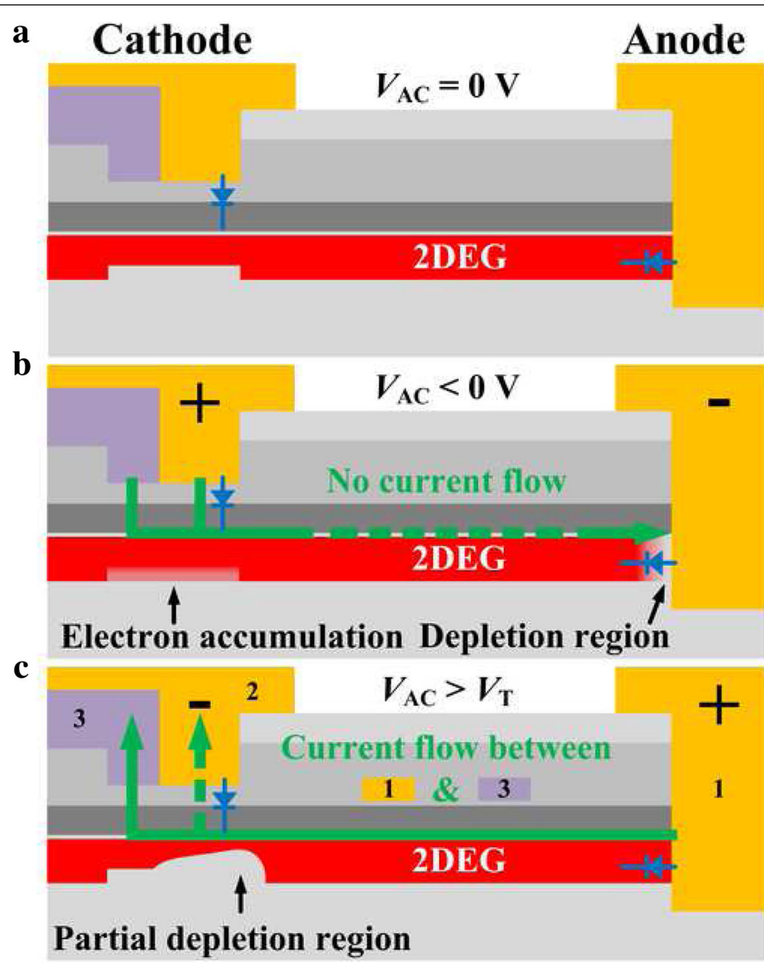

Fig. 4 Schematic operation mechanism of the RB-CRD under **a** zero bias, **b** reverse bias, and **c** forward bias conditions

channel in the cathode trench region is always existing at zero bias.

Figure 4 illustrates the operation mechanism of the RB-CRD. When a zero bias is applied to the anode ($V_{AC} = 0$ V) (see Fig. 4a), the RB-CRD is analogous to a Schottky-drain depletion-mode HEMT with the gate-source electrodes connecting. When a negative bias is applied to the anode ($V_{AC} < 0$ V) (see Fig. 4b), the electrons will accumulate in the cathode trench region while the 2DEG channel will be depleted in the anode region due to the reverse biased Schottky junction. There is no desired current following between the anode and the cathode, and the RB-CRD acts as a reverse biased SBD. As shown in Fig. 4c, when a positive bias which is beyond the turn-on voltage (V_T, at 1 mA/mm) of the anode SBD is applied to the anode ($V_{AC} > V_T$), the electrons will flow between the ohmic contact in the cathode and the Schottky contact in the anode. Meanwhile, the Schottky junction in the cathode is reverse biased and the 2DEG channel under the Schottky contact will be gradually depleted with increasing the forward bias. Therefore, the output current will initially increase with the applied anode voltage and then gradually reach saturation. In such case, a steady output current can be obtained.

The temperature-dependent forward *I-V* characteristics of the RB-CRD on the wafer are shown in Fig. 5. As shown in Fig. 5a, for the RB-CRD, a knee voltage (V_K, at 80% of the steady regulating current) of 1.3 V is obtained which is higher than that of our previously reported CRDs (e.g., typical value 0.6 V) [20, 21]. This is due to the additional voltage drop (e.g., typical value 0.7 V) on the anode SBD of the RB-CRD. With the temperature increasing from 25 to 300 °C (see Fig. 5a), a negative shift in the V_T is observed, which can be explained by the thermionic emission model (i.e., lesser energy is needed for electrons to overcome the Schottky barrier at higher temperatures). The RB-CRD is capable of outputting a steady regulating current up to 200 V (see Fig. 5b), which is higher than the reported maximum operation voltage of the Si-based commercial CRDs [22–24]. At 25 °C, the regulating current ratio ($I_{200\ V}/I_{25\ V}$) of the proposed RB-CRD is 0.998 indicating that the output current is quite steady. Thanks to the intrinsic high-temperature operation capability of AlGaN/GaN platform, the RB-CRD exhibits negligible degradation in the steadiness of the I_A up to 200 V at temperatures as high as 300 °C. Meanwhile, with the temperature increasing from 25 to 300 °C, the forward I_A reduces from 31.1 to 23.1 mA/mm due to the decreased electron mobility at elevated temperatures, as shown in Fig. 5b. The temperature coefficients (α) of the regulating current at different temperature ranges can be calculated by the following formula

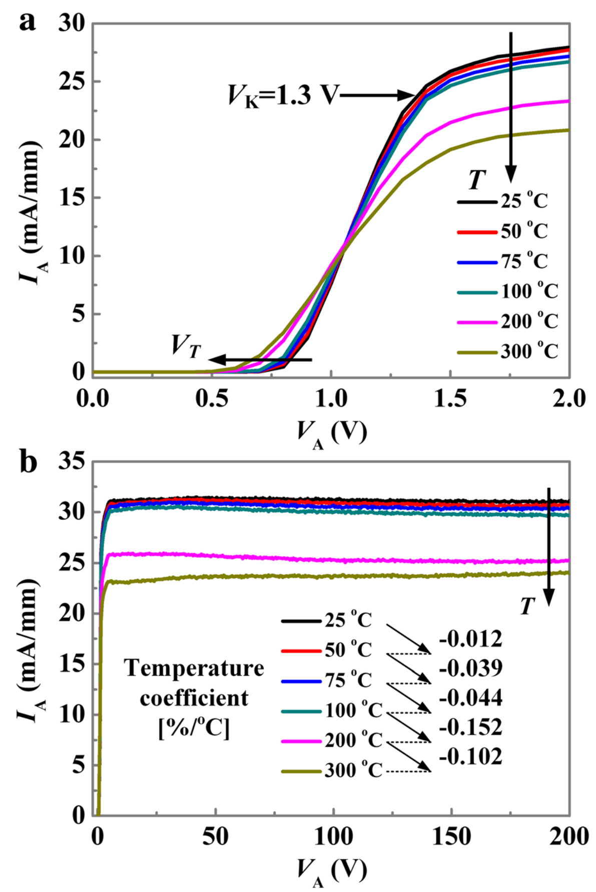

Fig. 5 Temperature dependent forward bias *I-V* characteristics of the RB-CRD. Anode voltage ranges: **a** 0–2 V, **b** 0–200 V

$$\alpha = \frac{I_1 - I_0}{I_0(T_1 - T_0)} \times 100\%$$

where I_0 is the output current at temperature T_0 and I_1 is the output current at temperature T_1. A small temperature coefficient less than −0.152%/°C is observed, indicating that the fabricated RB-CRD features excellent thermal stability.

As shown in the inset of Fig. 6, the reverse breakdown voltage of the RB-CRD is 260 V at 25 °C. The corresponding average critical electric field is calculated to be 0.65 MV/cm. The temperature dependent reverse *I-V* characteristics of the RB-CRD are shown in Fig. 6. The increase of the ambient temperature from 25 to 300 °C gives rise to an increase of the leakage current by two orders of magnitude.

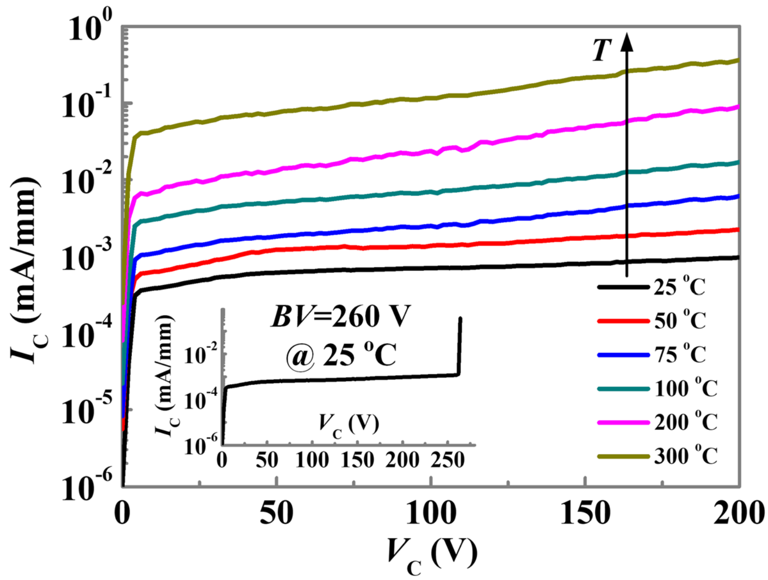

Fig. 6 Temperature dependent reverse bias *I-V* characteristics of the RB-CRD

Conclusions

In conclusion, a novel AlGaN/GaN-on-Si RB-CRD featuring trench Schottky anode and hybrid trench cathode has been successfully demonstrated for the first time. The fabricated RB-CRD exhibits a V_K of 1.3 V, a forward operation voltage over 200 V, and a reverse breakdown voltage of 260 V. An excellent accuracy as well as small negative temperature coefficient less than − 0.152%/°C have been obtained for the RB-CRD. The multifunctional RB-CRD with high accuracy is of great potential to be incorporated into emerging GaN power electronics systems.

Abbreviations

2DEG: Two-dimensional electron gas; AFM: Atomic force microscope; ICP: Inductively coupled plasma; MOCVD: Metal organic chemical vapor deposition; RB-CRD: Reverse blocking current regulating diode; SBD: Schottky barrier diode

Acknowledgements

Not applicable

Funding

This work was supported by the National Natural Science Foundation of China (No. 61674024), the Assembly Pre-research Project under Grant JZX2017–1643/Y537, the National Science and Technology Major Project of China (No. 2013ZX02308–005), the Opening project of State Key Laboratory of Electronic Thin Films and Integrated Devices under Grant KFJJ201609, and the Fundamental Research Funds for the Central Universities under Grant ZYGX2016J211.

Availability of Data and Materials

All data generated or analyzed during this study are included in this published article.

Authors' Contributions

AZ conceived and performed the experiments and the data analysis. BZ and QZ supervised this work. All authors discussed the results and contributed to the final manuscript. All authors read and approved the final manuscript.

Competing Interests

The authors declare that they have no competing interests.

Publisher's Note

Springer Nature remains neutral with regard to jurisdictional claims in published maps and institutional affiliations.

Received: 2 December 2018 Accepted: 8 January 2019
Published online: 15 January 2019

References

1. Mishra UK, Parikh P, Wu YF (2002) AlGaN/GaN HEMTs—an overview of device operations and applications. Proc IEEE 90(6):1022–1031
2. Ambacher O, Foutz B, Smart J, Shealy JR, Weimann NG (2000) Two dimensional electron gases induced by spontaneous and piezoelectric polarization in undoped and doped AlGaN/GaN heterostructures. J Appl Phys 87:334–344
3. Park PS, Nath DN, Krishnamoorthy S, Rajan S (2012) Electron gas dimensionality engineering in AlGaN/GaN high electron mobility transistors using polarization. Appl Phys Lett 100:063507
4. Pengelly RS, Wood SM, Milligan JW, Sheppard ST, Pribble WL (2012) A review of GaN on SiC high electron-mobility power transistors and MMICs. IEEE Trans Microw Theory Tech 60:1764–1783
5. Chow TP, Tyagi R (1994) Wide bandgap compound semiconductors for superior high-voltage unipolar power devices. IEEE Trans Electron Dev 41(8): 1481–1483
6. Im KS, Ha JB, Kim KW, Lee JS, Kim DS, Hahm SH, Lee JH (2010) Normally off GaN MOSFET based on AlGaN/GaN heterostructure with extremely high 2DEG density grown on silicon substrate. IEEE Electron Dev Lett 31:192–194
7. Ikeda N, Niiyama Y, Kambayashi H, Sato Y, Nomura T, Kato S, Yoshida S (2010) GaN power transistors on Si substrates for switching applications. Proc IEEE 98:1151–1161
8. Selvaraj SL, Ito T, Terada Y, Egawa T (2007) AlN/AlGaN/GaN metal–insulator–semicondutor high-electron-mobility transistor on 4 in. silicon substrate for high breakdown characteristics. Appl Phys Lett 90(17):173506
9. Huang S, Jiang Q, Yang S, Zhou C, Chen KJ (2012) Effective passivation of AlGaN/GaN HEMTs by ALD-grown AlN thin film. IEEE Electron Dev Lett 33(4):516–518
10. Cai Y, Zhou Y, Chen KJ, Lau KM (2005) High-performance enhancement-mode AlGaN/GaN HEMTs using fluoride-based plasma treatment. IEEE Electron Dev Lett 26:435–437

11. Zhou Q, Chen B, Jin Y, Huang S, Wei K, Liu X, Bao X, Mou J, Zhang B (2015) High-performance enhancement-mode Al_2O_3/AlGaN/GaN-on-Si MISFETs with 626 MW/cm^2 figure of merit. IEEE Electron Dev Lett 62:776–781
12. Zhou Q, Liu L, Zhang A, Chen B, Jin Y, Shi Y, Wang Z, Chen W, Zhang B (2016) 7.6 V threshold voltage high-performance normally-off Al2O3/GaN MOSFET achieved by interface charge engineering. IEEE Electron Dev Lett 37:165–168
13. Uemoto Y, Hikita M, Ueno H, Matsuo H, Ishida H, Yanagihara M, Ueda T, Tanaka T, Ueda D (2007) Gate injection transistor (GIT)—a normally-off AlGaN/GaN power transistor using conductivity modulation. IEEE Trans Electron Dev 54:3393–3399
14. Shih HY, Chu FC, Das A, Lee CY, Chen MJ, Lin RM (2016) Atomic layer deposition of gallium oixide films as gate dielectrics in AlGaN/GaN metal–oxide–semiconductor high-electron-mobility transistors. Nanoscale Res Lett 11:235
15. Wei J, Liu S, Li B, Tang X, Lu Y, Liu C, Hua M, Zhang Z, Tang G, Chen KJ (2015) Low on-resistance normally-off GaN double-channel metal-oxide-semiconductor high-electron-mobility transistor. IEEE Electron Device Lett 36:1287–1290
16. Liao WC, Chen YL, Chen ZX, Chyi JI, Hsin YM (2014) Gate leakage current induced trapping in AlGaN/GaN Schottky-gate HFETs and MISHFETs. Nanoscale Res Lett 9(1):474
17. Cope RC, Podrazhansky Y (1999) The art of battery charging. In: Proc. IEEE 4th Annu Battery Conf Appl Adv, pp 233–235
18. Zhang SS (2006) The effect of the charging protocol on the cycle life of a Li-ion battery. J Power Sources 161(2):1385–1391
19. Patnaik L, Praneeth AVJS, Williamson SS (2019) A closed-loop constant-temperature constant-voltage charging technique to reduce charge time of lithium-ion batteries. IEEE Trans Ind Electron 66(2):1059–1067
20. Zhang A, Zhou Q, Shi Y, Yang C, Shi Y, Yang Y, Zhu L, Chen W, Li Z, Zhang B (2018) AlGaN/GaN lateral CRDs with hybrid trench cathodes. IEEE Trans Electron Dev 65:2660–2665
21. Zhang A, Zhou Q, Chen W, Shi Y, Li Z, Zhang B (2017) An AlGaN/GaN current regulating diode. In: 29th International Symposium on Power Semiconductor Dev and IC's (ISPSD). Sapporo: IEEE; pp 203–206
22. Current regulator diodes (2004) Document 70195. VISHAY. Datasheet. available: http://www.vishay.com
23. Current regulating diodes (2011) Document T4-LDS-0160. Microsemi. Datasheet. available: https://www.microsemi.com/existing-parts/parts/57992
24. Current regulating diode (2017) Document P22–23-CRD. SEMITEC. Datasheet. available: http://www.semitec.co.jp/uploads/english/sites/2/2017/03/P22-23-CRD.pdf